Structure and magnetic order of the Heusler compound Co_2NbSn

A. U. B. Wolter,[1] A. Bosse,[1] D. Baabe,[1] I. Maksimov,[1] D. Mienert,[1] H. H. Klauß,[1] F. J. Litterst,[1] D. Niemeier,[2] R. Michalak,[3] C. Geibel,[3] R. Feyerherm,[4] R. Hendrikx,[5] J. A. Mydosh,[5] and S. Süllow[1]

[1]*Institut für Metallphysik und Nukleare Festkörperphysik, TU Braunschweig, 38106 Braunschweig, Germany*

[2]*Institut für Physikalische und Theoretische Chemie, TU Braunschweig, 38106 Braunschweig, Germany*

[3]*Max-Planck-Institut für Chemische Physik fester Stoffe, 01187 Dresden, Germany*

[4]*Hahn-Meitner-Institut GmbH, 14109 Berlin, Germany*

[5]*Kamerlingh Onnes Laboratory, Leiden University, 2300 RA Leiden, The Netherlands*

(Received 26 March 2002; revised manuscript received 2 July 2002; published 15 November 2002)

We present a detailed study of the structural and magnetic phase transitions of the Heusler compound Co_2NbSn. This material undergoes a structural transition at $T_S = 235$ K from the cubic Heusler $Fm3m$ high-temperature phase into an orthorhombic low-temperature lattice of $Pmma$ symmetry. Further, the system exhibits a magnetic transition at $T_C = 116$ K from para- to ferromagnetism. While on a macro- and mesoscopic scale Co_2NbSn appears to be fully $Fm3m$ ordered, from microscopic studies we find that on an atomic scale site disorder is present. We discuss the implications of these findings for the anomalous macroscopic physical properties and domain formation in the ferromagnetic state in Co_2NbSn.

DOI: 10.1103/PhysRevB.66.174428 PACS number(s): 75.60.Nt, 72.15.Eb, 75.50.Cc, 71.20.Be

I. INTRODUCTION

In recent years shape memory alloys have been subject to extensive research efforts due to their potential for technical applications.[1,2] In particular, ferromagnetic shape memory alloys have been studied intensively because of the possibility to control the shape memory effect (SME) by application of magnetic fields.[3–5] The prototype ferromagnetic shape memory alloy is Ni_2MnGa.[6] It orders ferromagnetically at $T_C \sim 350-380$ K, while the martensitic phase transition at T_S connected to the SME very strongly depends on the actual stoichiometry of the sample, varying between 200 and 400 K.[3,5–8] Depending on if the martensitic transition takes place in the ferro- or paramagnetic phase, different martensitic transitions arise, with a rich variety of SME.

On basis of band structure calculations Co_2NbSn has been argued to be closely related to Ni_2MnGa.[9] In previous investigations it has been established that the material undergoes a structural transition at $T_S \sim 200-250$ K and a ferromagnetic at $T_C \sim 100-120$ K with a small ordered moment of $0.3\mu_B$.[10–12] The character of the ferromagnetic state is itinerant, as is indicated by magnetic circular dichroism experiments.[12] Based on unpublished data of the alloying series $(Co_{1-x}Ni_x)_2NbSn$ it has been claimed that the structural and magnetic transition temperatures are suppressed to zero temperature at the same Ni concentration $x = 0.3$, which would indicate a very strong interlocking of the two phenomena.[9] As the driving mechanism behind the structural transition a band Jahn-Teller effect has been proposed.[9,11]

A striking feature of Co_2NbSn is the very strong sample dependence of its physical properties. Sample-to-sample variations of transition temperatures by 20 K (T_C) and 50 K (T_S) are observed.[9–11,13] In the most exhaustive study to date, Ref. 11, in none of the bulk properties (susceptibility χ, specific heat c_p, resistivity ρ) could T_C and T_S unambiguously and consistently be defined. Moreover, a resistivity ratio $\rho_{300\,K}/\rho_{4.2\,K} = 1$ and a negative temperature derivative $d\rho/dT$ over a wide temperature range are observed. This is in conflict with a fairly large density of states at the Fermi level, as derived from the electronic specific heat coefficient γ.[11,13] Further, at the first-order transition at T_S the accompanying specific heat anomaly is smeared out over a wide temperature range of 60 K. Such behavior points to the presence of crystallographic disorder, which, however, has not been identified so far; nor has its relevance for the electronic and magnetic properties been studied.

In view of these open issues we have reinvestigated Co_2NbSn. We have thoroughly characterized polycrystalline material by means of macro- and microscopic experiments, thus establishing the *intrinsic* properties of this compound. Complementarily, we have studied the local symmetry of Co_2NbSn by means of nuclear magnetic resonance (NMR) and Mössbauer spectroscopy. From these studies we find that Co_2NbSn is disordered on an atomic scale. We propose that the disorder accounts for the unusual magnetothermal hysteresis in Co_2NbSn, causing the formation of very narrow domain walls.

II. EXPERIMENTAL DETAILS

Polycrystalline samples Co_2NbSn have been prepared by arc melting the constituents (Co: 3N; Nb: 3N; Sn: 5N) in stoichiometric ratio under Ar atmosphere in a water-cooled copper crucible. Subsequently, the samples were annealed in evacuated quartz tubes at 850°C for 7 days.[14] The structure and homogeneity of the samples have been checked by x-ray and neutron diffraction. The samples are single phase and crystallize in the fully ordered $Fm3m$ Heusler structure at room temperature, with a lattice parameter of $a = 6.1526(3)$ Å. Comparison of this value to those reported in the Refs. 10, 11, and 15 reveals significant sample-to-sample variations, with the absolute values a of our samples consistently larger than those of the previous reports. It reflects a strong sample dependence even of the structural parameters. In Ref. 11 the sample has been quenched in water

after the heat treatment,[16] which likely gives rise to frozen-in disorder and possibly causes the observed variation of the lattice parameters.

The specific heat measurement was performed using a standard adiabatic heat-pulse technique in zero field between 10 and 300 K. The magnetic susceptibility was measured employing a commercial superconducting quantum interference device (SQUID) magnetometer, at temperatures ranging from 5 to 300 K in fields up to 5 T. Resistivity measurements were carried out by means of a standard ac four-point technique at temperatures ranging from 20 to 300 K. Powder neutron diffraction studies have been executed at the E9 spectrometer of the HMI, with an incident neutron wavelength $\lambda = 1.581\,92(5)$ Å. Temperature-dependent x-ray diffraction experiments have been carried out between 10 and 300 K. For the room-temperature ^{119}Sn Mössbauer experiments a $Ca^{119m}SnO_3$ source was used in conventional transmission geometry in connection with a scintillation counter.

Muon spin resonance (μSR) experiments in zero external field (ZF) and longitudinal external field (LF) (parallel to the initial muon spin polarization) have been performed between 3 and 290 K at the M20 beamline of the TRIUMF muon facility. The powderized sample Co_2NbSn was mounted in a low-background sample environment using ultrathin aluminum tape. To deduce the time dependence of the muon spin polarization the count rates in two positron detectors mounted upstream and downstream of the muon beam were analyzed using the corrected asymmetry method.[17] A 20 G transversal field experiment at 290 K was used to calibrate the base line. It could be fitted with a signal amplitude (initial asymmetry) of $A_0 = 0.197(1)$ and a single Gaussian relaxation of $\sigma = 0.157(2)$ μs^{-1}. Due to the low-background setup the full asymmetry can be assigned to the Co_2NbSn sample. The signal amplitude was kept fixed for the analysis of the ZF and LF experiments.

NMR measurements were performed with a modified Bruker pulse spectrometer in quadrature detection and a superconducting magnet operating at magnetic fields up to $B = 7.05$ T at temperatures between 31 and 293 K. The exact value of the field for the Knight shift measurements has been determined via the resonance frequency of ^{59}Co in a $K_3Co(CN)_6$ aqueous solution. For the NMR, neutron scattering, x-ray diffraction, and Mössbauer experiments Co_2NbSn has been powderized in a mortar. Because of the powdered sample, the NMR responses of the ^{59}Co and ^{93}Nb nuclei are distributed over a wide frequency range, causing a decrease in the signal-to-noise ratio. For the NMR measurements, the sample was placed in a glass tube which showed no observable NMR signals in the ^{59}Co and ^{93}Nb frequency range.

III. RESULTS AND DISCUSSION

In Fig. 1 we present the neutron diffraction spectra of Co_2NbSn measured at 300 and 5 K. Full Rietveld structure refinements have been carried out employing the program WINPLOT/FULLPROF.[18] The results of the fitting procedure are summarized in Table I. At room temperature the spectrum is best described assuming the $L2_1$ structure, i.e., a Heusler lattice with $Fm3m$ symmetry.[10,11] Within experimental resolution (5%) there is no evidence for site exchange of Co, Nb, and Sn atoms on equivalent sites. At 5 K the material has transformed into a low-temperature phase of reduced symmetry. Following Ref. 11 we refine our data assuming an orthorhombic $Pmma$ unit cell for the low-temperature phase. Our refinement is in full agreement with that of Ref. 11.

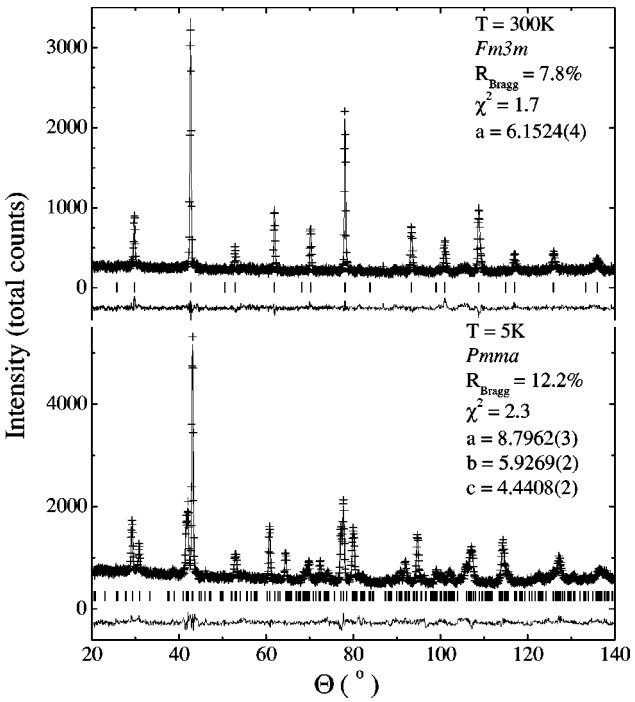

FIG. 1. The neutron diffraction spectra of Co_2NbSn in the cubic $Fm3m$ phase at 300 K and orthorhombic $Pmma$ phase at 5 K. Tics indicate Bragg peak positions, (+) represents experimental data, and the result of the refinement and the difference between refinement and fit are plotted as solid lines.

TABLE I. The refinement results of the neutron diffraction spectra, including positional parameters *x*, *y*, *z* of the $Pmma$ lattice of Co_2NbSn.

	$Fm3m_{300\,K}$	$Pmma_{100\,K}$	$Pmma_{5\,K}$
a (Å)	6.1524(4)	8.7932(3)	8.7962(3)
b (Å)	-	5.9432(2)	5.9269(2)
c (Å)	-	4.4356(2)	4.4408(2)
B_{iso}	0.82(9)	0.56(9)	0.44(9)
χ^2	1.7	2.4	2.3
R_{Bragg} (%)	7.8	11.8	12.2
	x	*y*	*z*
Co (4*h*)	0	0.253(40)	$\frac{1}{2}$
Co (4*k*)	$\frac{1}{4}$	0.746(33)	0.051(5)
Nb (2*a*)	0	0	0
Nb (2*f*)	$\frac{1}{4}$	$\frac{1}{2}$	0.527(15)
Sn (2*e*)	$\frac{1}{4}$	0	0.537(17)
Sn (2*b*)	0	$\frac{1}{2}$	0

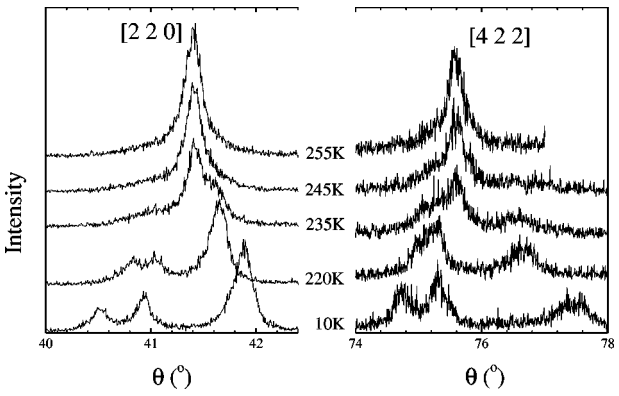

FIG. 2. The temperature dependence of the [2 2 0] and [4 2 2] peaks upon transition from the cubic high-temperature to orthorhombic low-temperature phase.

By comparing the B_{iso} values in the cubic and orthorhombic phases we determine the effect of the structural transition on the lattice properties. Assuming at 100 and 300 K the validity of the high-temperature limit of the Debye model, i.e., that the mean-square displacement can be expressed as $\langle x^2\rangle = 3\hbar T/Mk_B\Theta_D^2$, we evaluate the ratio $\Theta_{D,300\ \mathrm{K}}/\Theta_{D,100\ \mathrm{K}} = 1.4$. Thus, the structural transition from the cubic to orthorhombic phase causes a substantial softening of the lattice.

In Fig. 2 we plot the T dependence of the [2 2 0] and [4 2 2] peaks, determined from x-ray diffraction. Upon lowering the temperature below $T_S = 235 \pm 5$ K both peaks split up into three separate peaks in the orthorhombic cell. In Fig. 3 we plot the T-dependent lattice parameters. Note that in order to compare distances in the low- and high-temperature phases we plot the values $\sqrt{2}a$, b, and $c/\sqrt{2}$ for the orthorhombic lattice, normalized by the cubic lattice parameter a at 300 K. The structural transition gives rise to a large variation of interplanar distances up to 4%, compared to the cubic lattice. In contrast, the volume of the unit cell $V = a \times b \times c$ remains almost constant over the whole temperature range.

The magnetic properties of Co_2NbSn are summarized in the Figs. 4 and 5. In Fig. 4 we plot the T dependence of the

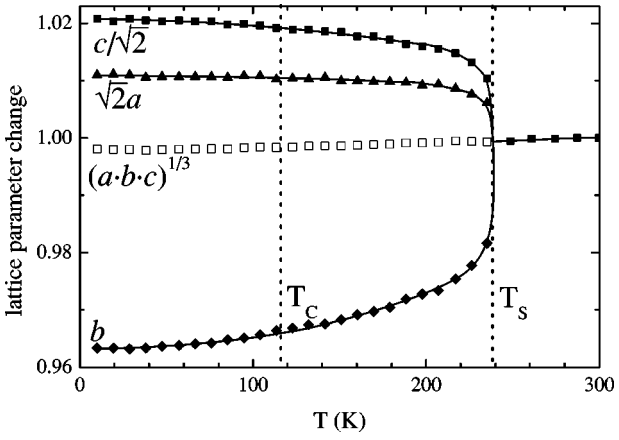

FIG. 3. The temperature dependence of the lattice parameters of $Fm3m$ and $Pmma$ Co_2NbSn, normalized by the room-temperature value.

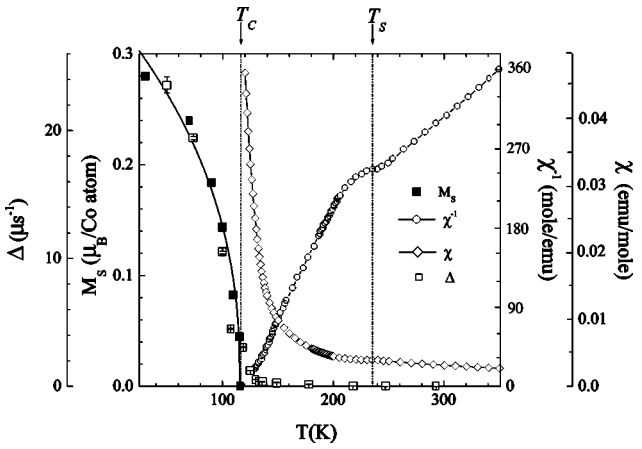

FIG. 4. The T dependence of the susceptibility χ, inverse susceptibility χ^{-1}, and spontaneous magnetization M_S of Co_2NbSn. We include the relaxation rate Δ, obtained in a μSR experiment, which demonstrates the scaling of Δ with M_S.

spontaneous magnetization M_S, determined from an Arrot plot analysis, the susceptibility χ, and inverse susceptibility χ^{-1} (for details see Ref. 19). We include the width of the static internal field distribution Δ, obtained via μSR (see below). From $M_S(T)$ we determine the Curie temperature to $T_C = 116 \pm 2$ K. The ordered magnetic moment approaches $0.3\mu_B$/Co atom at low temperatures (Figs. 4 and 5). The solid line in Fig. 4 represents a fit $M_S \propto (T_C - T)^\beta$, $\beta = 0.42$, indicating a tendency towards mean-field-like behavior. The coercitivity of the material is comparatively large for an itinerant magnet ($\sim$0.15 T). The field evolution of the virgin curve of the magnetization implies that the coercitivity is pinning controlled (Fig. 5).[20]

In the cubic phase the susceptibility follows a Curie-Weiss behavior, with $\mu_{eff} = 1.35\,\mu_B$/Co atom and $\Theta_{CW} = -7$ K. Thus, for the cubic structure the magnetic coupling

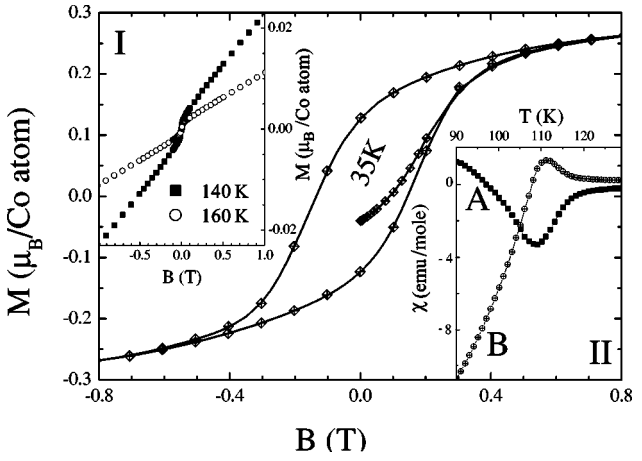

FIG. 5. A hysteresis loop of Co_2NbSn at 35 K. Inset I demonstrates the presence of a small ferromagnetic signal above T_C. Inset II represents the pronounced magnetothermal hysteresis. *A* corresponds to an experiment with the sample cooled in -32 G and measured in $+50$ G, *B* to a cooling in $+8$ G and measurement in -50 G.

is weakly antiferromagnetic, in contrast to the ferromagnetic coupling in orthorhombic symmetry. The structural transition into the orthorhombic lattice is visible as a kink-type minimum in χ^{-1}, from which we determine $T_S = 233 \pm 3$ K.

Below the structural transition the magnetic behavior is complex. On the one hand, χ^{-1} is linear between 150 and 210 K. In the magnetization, however, we observe an S-shaped magnetization and magnetic hysteresis above T_C, pointing to the presence of a ferromagnetic phase (inset I, Fig. 5). From a μSR study (see below) we conclude that the signal arises from a minority phase. The ferromagnetic signal of the minority phase disappears at about T_S, and therefore we have not determined Curie-Weiss parameters in this temperature range.

In addition, there is a complicated history dependence of the magnetization in the ferromagnetic regime.[19] Cooling the sample in the remnant field of a superconducting magnet and measuring it in a field directed opposite to the remnant field causes a temperature dependence of χ as depicted in inset II of Fig. 5. This behavior resembles that observed in certain rare-earth-transition metal alloys like $SmNi_4B$,[21] $Pr_2Fe_{17-x}Mn_x$,[22] or $ThCo_{5x}Ni_{5-5x}$ compounds.[23,24] It is attributed to the formation of very narrow domain walls forming in the ferromagnetic state even in an itinerant magnet.

Further, we have performed μSR experiments on Co_2NbSn. Below T_C the ZF and LF μSR spectra exhibit a strong static electronic relaxation. The spectra could be fitted using a Kubo-Toyabe function derived for an isotropic Lorentzian field distribution in a powder sample (Fig. 6). Hence, the material is homogeneously magnetically ordered. A well-defined spontaneous muon spin precession is not observed. The limited quality of the fit using a Lorentzian field distribution centered at $B=0$ T may be explained assuming a finite local field $\langle B \rangle$ at the muon site with a broad distribution $\langle \Delta B \rangle$. The static relaxation rate $\Delta(T=2\ \mathrm{K}) \approx 30\ \mu s^{-1}$ results in an internal field distribution of width $\langle \Delta B \rangle \approx 350$ G at the muon site. In the cubic Heusler crystal structure two possible muon sites of octahedral coordination exist at positions (0.5, 0, 0.25) (site a) and (0.25, 0, 0.25) (site b). Dipole field calculations assuming a magnetic moment of $0.3\mu_B$ at the Co atoms result in local fields between 0.5 and 1 kG (site a) or 1.5 and 3 kG (site b) depending on the spatial alignment of the ferromagnetic moments. Only for a muon site of tetrahedral coordination (0.125, 0.25, 0) (site c) and a spin alignment parallel to (1, 0, 0) directions an internal field of 0.26 kG is found. However, it should be emphasized that additional Fermi contact hyperfine fields are not included in these calculations and may alter the determination of the actual muon site and spin orientation.

The scenario of an overdamped muon spin precession is explained by local muon site disorder. Below T_S the symmetry at all muon sites is reduced and different environments are formed by atomic displacements in the low-temperature phase. These displacements give rise to a distribution of local fields in the magnetically ordered regime. A quantitative calculation is difficult since the presence of the muon in the lattice leads to an additional site relaxation of the atomic positions of the same order of magnitude. Therefore the additional disorder contribution to Δ caused by local impurities

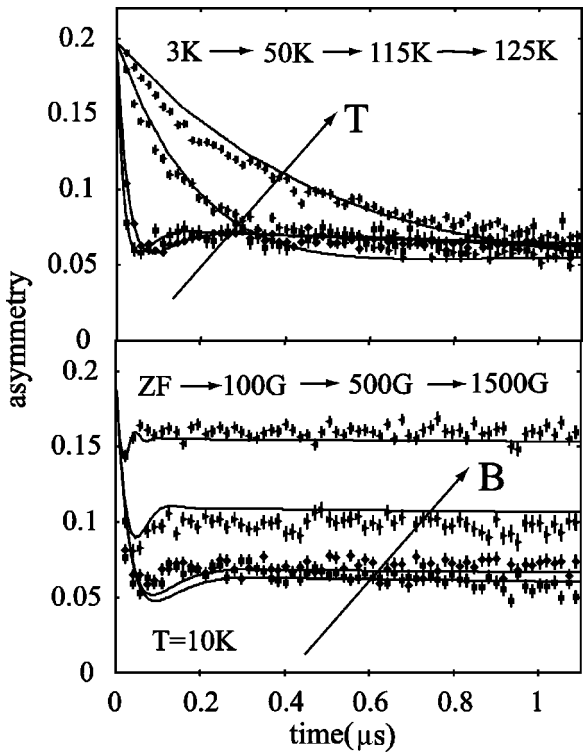

FIG. 6. Typical zero field (ZF) (upper panel) and longitudinal external field μSR (lower panel) spectra of Co_2NbSn for $T \leqslant T_C$.

cannot be extracted. The observed scaling of Δ with the macroscopic magnetization (Fig. 4) is consistent with the discussed line broadening effects.

Above $T_S = 235$ K the ZF μSR spectra of Co_2NbSn can be fitted by a product of a simple exponential relaxation and a static Gaussian Kubo-Toyabe-type function,

$$G_z(t) = A_0 \exp(-\lambda t)\left[\frac{1}{3} + \frac{2}{3}(1-\sigma^2 t^2)\exp\left(-\frac{1}{2}\sigma^2 t^2\right)\right]$$

(σ=width of static Gaussian field distribution) (Fig. 7). The exponential term describes a relaxation due to electronic moments; the Kubo-Toyabe term accounts for the relaxation due to static nuclear moments.

At 290 K, a longitudinal field of 100 G is sufficient to suppress the muon spin depolarization due to nuclear magnetic moments [Fig. 7(a)]. As the temperature is lowered below $T_S = 235$ K, the spectra are qualitatively changed [Figs. 7(b) and (c)]. LF experiments prove the quasistatic nature of the electronic relaxation, since at 162 K and 123 K only a partial decoupling of the relaxation is achieved in LF fields ~ 100 G. Higher LF fields of ≈ 500 G are required to decouple the muon spin from the static internal fields, which due to their size have to be of electronic origin. Then, the relaxation processes cannot be regarded as independent and the above given product relaxation function is inappropriate. Therefore, all ZF spectra between 290 K and 120 K have been analyzed using a relaxation function derived for an isotropic static internal field distribution convoluted from a Gaussian and a Lorentzian field distribution (inset of Fig. 8):

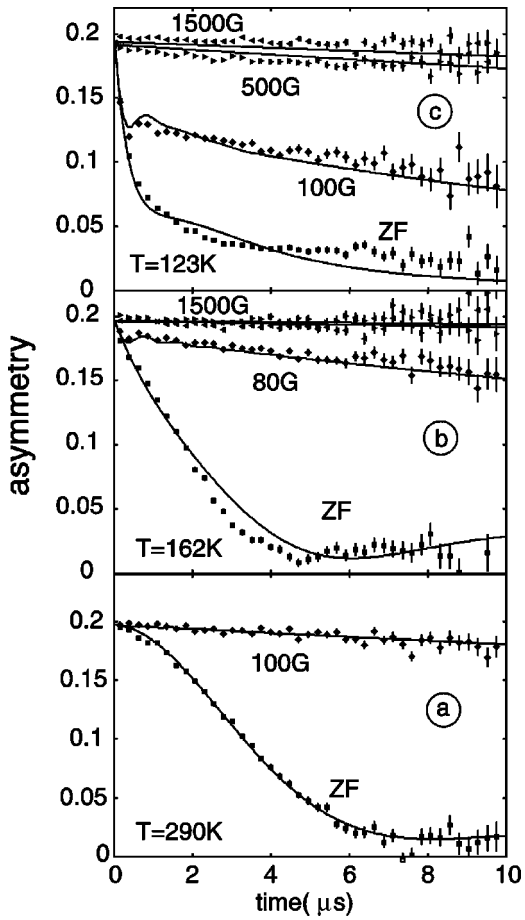

FIG. 7. ZF and LF μSR spectra of Co_2NbSn for $T>T_C$. At 123 and 162 K the spectra were analyzed using a two-component fit of a Gaussian and Lorentzian field distribution. At 290 K only a Gaussian field distribution is used.

$$G_z(t)=A_0\left[\frac{1}{3}+\frac{2}{3}(1-\Delta t-\sigma^2t^2)\exp\left(-\Delta t-\frac{1}{2}\sigma^2t^2\right)\right].$$

Here, the Lorentzian distribution of width Δ is ascribed to the electronic relaxation and the Gaussian distribution of width σ is due to the nuclear relaxation. Above T_S a nuclear damping of $\sigma=0.20(3)\ \mu s^{-1}$ is derived which increases to $0.28(2)\ \mu s^{-1}$ below the structural transition. The resulting T dependence of Δ and typical ZF spectra are shown in Fig. 8. The narrow static field distribution between T_S and T_C indicates the existence of highly diluted magnetic domains. The static width Δ is $\approx$100 times smaller than below T_C. Assuming a similar size of the magnetic moment per Co site as in the ferromagnetic phase the volume fraction of the magnetic domains can be estimated to a percent randomly distributed in the lattice. This is consistent with the ratio of the size of the spontaneous magnetic moment below and above T_C (about 1/100). Since a ferromagnetic signature is observed upon transition into the orthorhombic phase, it possibly indicates that the secondary magnetic phase is a derivative of cubic or orthorhombic Co_2NbSn, like, for instance, a strained phase in the grain boundaries.

Magnetic order and the structural transition are bulk phenomena, as established by the specific heat plotted in Fig. 9.

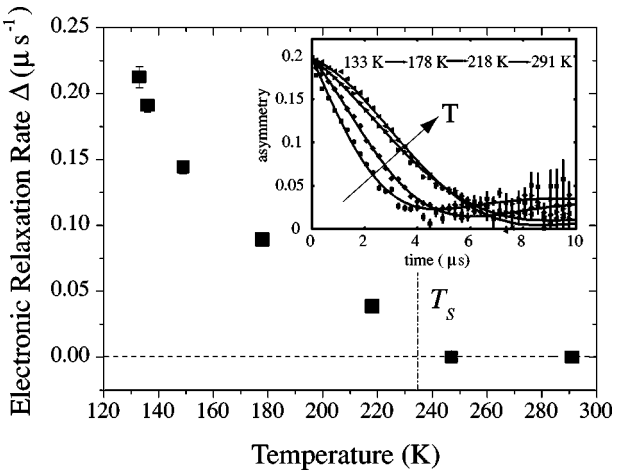

FIG. 8. Temperature dependence of the Lorentzian static width Δ of the local field distribution at the muon site above T_C. Inset: typical ZF time spectra fitted with a convoluted Gaussian and Lorentzian relaxation function.

At the structural transition a large anomaly is seen ($T_S=233$ K, from the maximum of the anomaly), attesting to the first-order nature of the transition. Compared to Ref. 11 the specific heat anomaly of our sample is much more pronounced and distributed over a much more narrow temperature range of 5 K. Moreover, for our sample the anomaly occurs at the temperature at which in x-ray diffraction the transition has been observed.

From Fig. 9 we determine the lattice specific heats for the high- and low-temperature phases by modeling them as Debye contributions. For this, we applied a fit with the full Debye integral calculated by an interpolation scheme to the corresponding temperature regimes.[25] We include an electronic specific heat $c_{p,el}=\gamma T$, $\gamma=26$ mJ/mol K^2.[13] With average Debye temperatures Θ_D of 365 K for the cubic and 275 K for the orthorhombic structure we reproduce the spe-

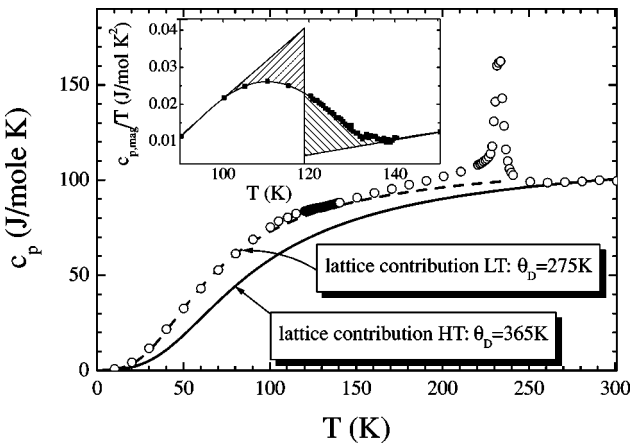

FIG. 9. The specific heat c_p of Co_2NbSn. The structural transition at $T_S=233$ K appears as a first-order transition; the ferromagnetic transition at $T_C\simeq120$ K is derived after subtracting a lattice contribution to c_p (inset). The lattice contributions for the low- and high-temperature phases are indicated by dashed and solid lines; for details see text.

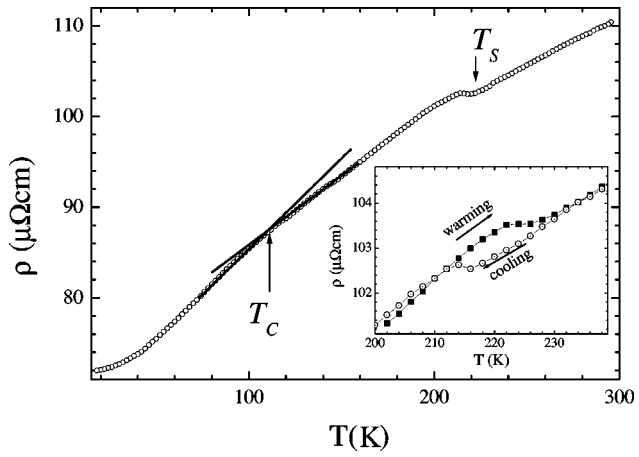

FIG. 10. The resistivity of Co_2NbSn as a function of temperature. The structural transition causes thermal hysteresis, as indicated in the inset.

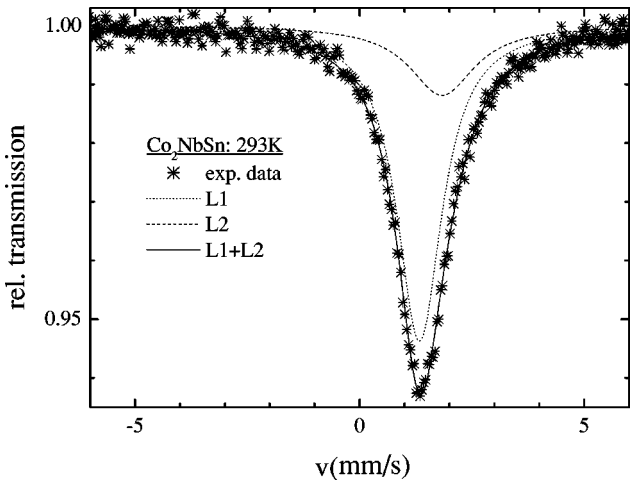

FIG. 11. Room temperature ^{119}Sn Mössbauer spectra of Co_2NbSn. Two Lorentz functions $L1$ and $L2$ are required to fit the spectrum; for details see text.

cific heat far above T_S and below T_C, respectively (dashed and solid lines in Fig. 9). We calculate the ratio of the Debye temperatures, $\Theta_{D,\mathrm{cubic}}/\Theta_{D,\mathrm{ortho}}=1.3$, a value consistent with that obtained via the B_{iso} values from neutron scattering, thus supporting the notion of a softening of the lattice at the structural transition.

By subtracting the combined specific heat contributions from phonons and electrons, $c_{p,phonon}+c_{p,el}$, from the total specific heat c_p for the low-temperature phase we determine the magnetic specific heat $c_{p,mag}$. In the inset of Fig. 9 we plot $c_{p,mag}/T$ as a function of T, revealing a second-order phase transition at T_C. From an entropy balance construction—i.e., the striped triangular areas in the inset of Fig. 9 are required to be of equal size—we determine $T_C \simeq 119$ K. From this construction we estimate the size of the specific jump $\Delta c_{p,mag}$ at T_C, which we evaluate to about 4 J/mol K. This value is much smaller than that expected for an ordering transition of Co^{2+} ions, which, depending on $J=S$ or $L+S$, would yield values $\Delta c_{p,mag}\simeq 18$ and 20 J/mole K, respectively. Correspondingly, the entropy released in the ferromagnetic transition, $S=0.17R\ln(2)$, is much smaller than expected for an ordering transition of localized Co^{2+} moments. Both observations reflect the itinerant nature of ferromagnetism in Co_2NbSn.

The resistivity ρ of Co_2NbSn as function of temperature is plotted in Fig. 10. The overall resistive behavior is metallic, although a comparatively large absolute value of ρ and a small $\rho_{300\,\mathrm{K}}/\rho_{20\,\mathrm{K}}=1.5$ is indicative of remnant strain or disorder. At the structural transition a small upward jump is detected in ρ, which exhibits hysteresis upon cycling the temperature.[14] This is illustrated in the inset of Fig. 10, where we show an enlarged view of the transition region, with ρ during a cooling-warming cycle through the transition. Further, the signature of the ferromagnetic transition is a change of resistive slope at ~ 112 K, visualized by the line construction. A weak signature of T_C in the resistivity is expected for this type of magnet, as within fluctuation theory it is predicted that $d\rho/dT \propto c_p$.[26,27] Hence, the change of slope depends on the size of the ordered moment, which in Co_2NbSn is small.

Our resistivity experiment stands in marked contrast to that of Ref. 11. This reflects different levels of crystallographic disorder in the investigated samples. For our sample the small resistivity ratio $\rho_{300\,\mathrm{K}}/\rho_{20\,\mathrm{K}}$ indicates the presence of strain or disorder. The level of disorder is even larger in the sample of Ref. 11, as $\rho_{300\,\mathrm{K}}/\rho_{20\,\mathrm{K}}$ is smaller; there is neither an unambiguous signature of T_S nor T_C, and ρ exhibits a negative temperature derivative $d\rho/dT$ over a wide temperature range. The resistivity of Ref. 11 resembles that of strongly disordered metals, in which electronic transport is approaching the diffusive limit.[28]

Similarly, the other bulk properties validate our claim of a higher crystalline quality of our samples compared to that of Ref. 11. For our samples we observe T_S in the susceptibility, the width of the specific heat anomaly at T_S is smaller by an order of magnitude, and the ferromagnetic ordering is detected in c_p. The crystalline quality of Co_2NbSn appears to be mainly a function of the annealing procedure, as both the magnetic and structural transition temperatures T_S and T_C depend strongly on it. The values of T_S and T_C are about 20–30 K higher for annealed than for as-cast samples.[14]

In contrast to the pronounced sample dependencies arising from disorder, in our structural investigation we found perfect agreement with previous studies[11] and no indication of crystallographic disorder. Thus, disorder must be realized on an atomic scale, which is hard to detect in diffraction techniques. To study the local symmetry in Co_2NbSn we have employed microscopic techniques.

Direct evidence for crystallographic disorder on an atomic scale in Co_2NbSn comes from Sn Mössbauer experiments on the cubic room-temperature phase. Here, a single, broad absorption line is observed (Fig. 11). To fit the spectrum at least two Lorentzian lines $L1$ and $L2$ are required, with isomer shifts IS's and line widths Γ [full width at half maximum (FWHM)] of IS=1.83(28) mm/s; $\Gamma=1.77(14)$ mm/s ($L1$) and IS=1.33(3) mm/s; $\Gamma=1.22(7)$ mm/s ($L2$). From the integrated intensities we obtain relative weights of 24% for $L1$ and 76% for $L2$, implying a 1:3 distribution of local Sn environments. The values Γ are fairly large, compared to

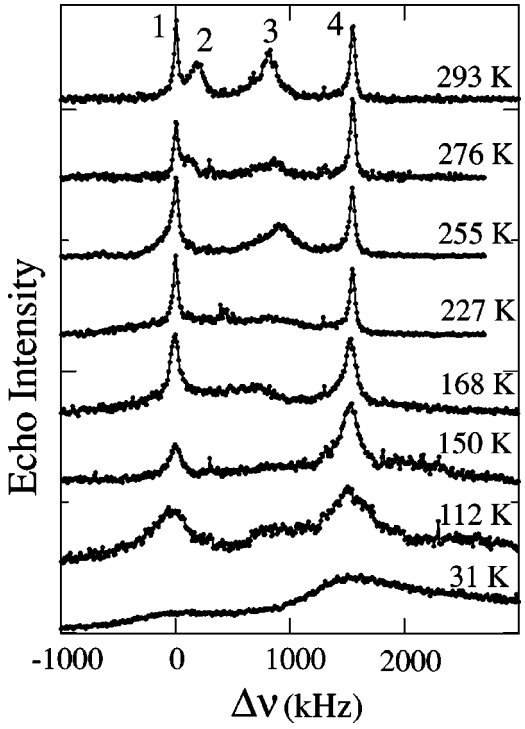

FIG. 12. The ^{59}Co and ^{93}Nb NMR signals as a function of temperature.

isostructural Co_2ScSn,[29] suggesting that both local Sn environments represent an average response from different configurations.

To further study the structural disorder in Co_2NbSn we performed ^{59}Co and ^{93}Nb NMR experiments. Broad frequency spectra of ^{59}Co and ^{93}Nb were obtained using an echo sequence, $\pi/2$-τ-π-τ-acq, with phase cycling which efficiently canceled any transmitter pulse breakthrough.[30,31] Typical conditions of excitation were $\pi/2=8\ \mu$s and $\pi=16\ \mu$s for a 90° and 180° pulse and $\tau=50\ \mu$s, respectively. Repetition rates were in the range 0.05–0.5 kHz. The NMR spectra were recorded piecewise by 50 kHz sections using Fourier transform NMR at 4.64 T and summation over the frequency range 45.7–49.7 MHz. The ^{59}Co NMR shift was determined using an aqueous $K_3Co(CN)_6$ solution as a reference, while the ^{93}Nb shift was determined with respect to the ^{59}Co reference frequency ν_R by $\nu_R\times(^{93}\gamma_n/^{59}\gamma_n)$ (γ=gyromagnetic ratio) with the tabulated values of $^{59}\gamma_n=2\pi\times10.054$ MHz/T and $^{93}\gamma_n=2\pi\times10.407$ MHz/T.

The main experimental observation is presented in Fig. 12, where we plot the NMR spectra of $I=7/2$ ^{59}Co and $I=9/2$ ^{93}Nb as function of temperature. In this figure zero frequency is associated with the ^{59}Co reference of aqueous $K_3Co(CN)_6$. At room temperature, in a perfect $Fm3m$ structure, Co and Nb each would occupy only one crystallographic site, giving rise to two lines in the NMR spectrum. Instead, we observe four lines, labeled 1–4. It either implies (a) two inequivalent sites in the lattice occupied by Co and Nb ions each or (b) a quadrupolar splitting of the Co and Nb signal even in cubic symmetry.

For quadrupolar splitting the frequency shift between two lines adheres to $\nu=\gamma B(1+K)+\nu_Q$ (K=Knight shift, ν_Q=quadrupole resonance frequency), implying that, for $B\rightarrow0$, $\nu=\nu_Q neq 0$. Thus, to test scenario (b) we determined the field dependence of the NMR spectra. In Fig. 13 we plot the frequency shift $\Delta\nu_1$ of lines 2–4 with respect to line 1 as a function of B. The shifts vary linearly with field and extrapolate to zero, excluding a quadrupolar splitting as source for the four lines.

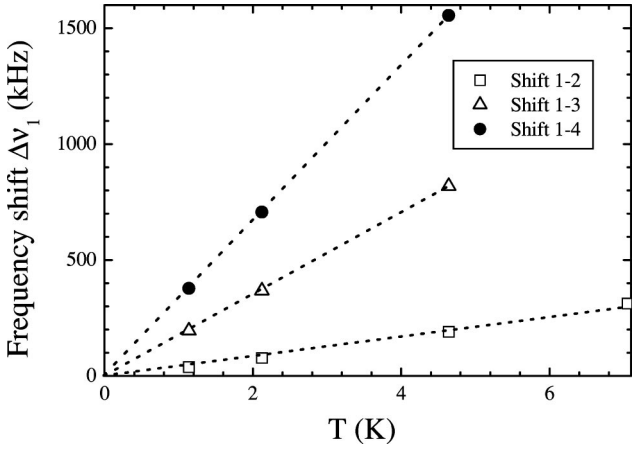

FIG. 13. The field dependence of the shifts of lines 2, 3, and 4 of Co_2NbSn with respect to line 1, $\Delta\nu_1$.

Since line 1 lies close to that of free ^{59}Co and line 4 to the ^{93}Nb signal, we associate them accordingly. In Fig. 14 we plot the T dependence of the Knight shift and linewidth (FWHM) of lines 1 and 4. The structural transition is discernable in the Knight shift of line 4, which above T_S is nearly constant, while between T_S and T_C it falls off linearly. It reflects the fact that the value of the Knight shift of ^{93}Nb above T_S is determined by both the transferred hyperfine field from the Co ion and dipolar contributions. Below T_S, with a reduced symmetry, dipolar contributions are modified, causing the T dependence of the Nb Knight shift. For line 1 no feature is seen at T_S, which is the consequence of the

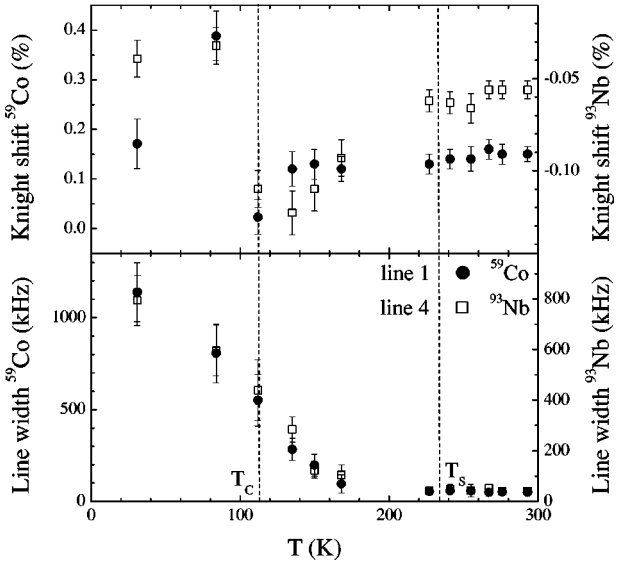

FIG. 14. The temperature dependence of Knight shift and linewidth of Co_2NbSn.

hyperfine field being the dominant term for the Knight shift of ^{59}Co at all temperatures, as Co carries the magnetic moment. Upon reduction of T below T_C both lines exhibit a rapid change of the Knight shift because of an increasing hyperfine field.

The T dependence of the linewidth (FWHM) mirrors the internal field and field distributions (Fig. 14). Hence, no anomaly is seen at T_S for lines 1 and 4, while upon approaching T_C both lines are broadened. The onset of a magnetic signature in the linewidth occurs at about 160 K. The discrepancy with the bulk T_C value probably arises from the secondary magnetic phase, which gives rise to the anomalous magnetization above T_C and quasistatic signature of the μSR spectra (see above). The internal field distribution at 30 K extracted from the FWHM data is determined to $\approx$1100 G and 770 G for the Co and Nb sites, respectively. The larger value for Co reflects the fact that it carries the magnetic moment. The size of the field distribution observed in NMR is in semiquantitative agreement with the μSR experiments (300 G at 30 K). Full quantitative agreement is not expected due to quadrupolar broadening of the NMR lines and the inequivalent crystallographic sites of Co, Nb, and the probing muon.

In contrast to the regular behavior of lines 1 and 4, lines 2 and 3 become very broad and shift substantially as the temperature is reduced. Because of the strong temperature dependence of their position and width, lines 2 and 3 cannot be unambiguously associated with Co or Nb; nor is an accurate determination of the Knight shift and linewidth possible.

Altogether, from our Mössbauer and NMR study we find that on a local scale Co_2NbSn is disordered, with two local environments, viz., configurations (referred to as $L1$ and $L2$), for each Co, Nb, and Sn even in the cubic $Fm3m$ structure. Because of their regular behavior, it is tempting to associate lines 1 and 4 in the NMR experiment with Co and Nb sited on the nominal positions of the $Fm3m$ and $Pmma$ lattice. Then, lines 2 and 3 correspond to Co and Nb ions randomly distributed on sites close to the nominal positions, giving rise to an incoherent response in local probe studies. Since the area below lines 2 and 3 is larger than below 1 and 4 (taking into account the larger T_2 times of lines 1 and 4), these lines correspond to the $L2$ configuration with 76% volume amount. The disorder on these sites must be realized as a small static displacement of the ions from the nominal positions of the $Fm3m$ and $Pmma$ lattices irresolvable in diffraction experiments. Because of the small displacements the two configurations $L1$ and $L2$ are almost degenerate energetically, and likely they are randomly distributed throughout the sample rather than being phase separated.

The disorder is nonintentional; i.e., in a stoichiometric intermetallic compound translational symmetry is broken.[32] In recent years a number of cases of nonintentional disorder have been reported, specifically for heavy fermion compounds.[33–36] For heavy fermions moderate levels of nonintentional disorder determine the ground-state properties. The effect of disorder in a metal with less strong electronic correlations like Co_2NbSn is not as dramatic, but still accounts for the anomalous behavior of the bulk properties and the pronounced sample dependences. In particular, it accounts for the observation of a nonmetallic resistivity and a first-order transition smeared out over 60 K in Ref. 11. The disorder level of the sample studied in that work is comparatively high, probably stemming from the fast quenching after the heat treatment. If the cooling procedure is a relevant element controlling the disorder level, it would suggest a structural instability of Co_2NbSn at high temperatures, giving rise to ions occupying on time average positions displaced from the high-symmetry sites, which are locked into their position in the cooling process. Then, with annealing and slow cooling the disorder level can be reduced.

In most cases, the prime effect of disorder on a band structure is to broaden the electron bands. In this situation, since in Co_2NbSn both the magnetic and structural transitions are considered to be band structure effects, a higher disorder level should coincide with lower values of T_S and T_C. This would explain the strong annealing dependence of the characteristic temperatures. To investigate this notion, improved band structure calculations either on fully ordered or disordered Co_2NbSn would be very useful for a deeper understanding of this material.

We believe that disorder plays an important role in the domain wall formation of Co_2NbSn. The occurrence of narrow domain walls in itinerant ferromagnets is unusual. Their formation requires an anisotropy energy K_1 of similar magnitude or larger than the magnetic exchange J, a condition hard to fulfill for itinerant magnets because of their comparatively small anisotropy energies ($K_1 \sim \frac{1}{100} - \frac{1}{10}$ MJ/m^3). Instead, narrow domain walls are typically observed in magnets with good local moments in anisotropic lattices, and/or under the influence of strong crystalline electric field (CEF) anisotropy ($K_1 \sim 1$–10 MJ/m^3).[20–24]

The anisotropy energy K_1 can be expressed as $K_1 = \frac{1}{2} H_A M_S$ (H_A anisotropy field).[24] M_S is a factor of 6 smaller than that of typical Co ferromagnets, and there is neither pronounced structural nor CEF anisotropy that could enhance H_A. On the other hand, T_C of Co_2NbSn is smaller by a factor 5–10 compared to such other itinerant Co ferromagnets, implying that the ratio K_1/J will be comparable to these systems. Thus, the intrinsic parameters yield no hint favoring narrow domain walls.

Instead, we believe that a ''pinninglike'' mechanism stemming from the structural disorder accounts for the formation of narrow domain walls in Co_2NbSn. The magnetic anisotropy energy will be different in the two local environments, causing a difference in domain wall energies γ: $\gamma(L1)$ and $\gamma(L2)$. Then, the magnetostatic energy contains a term $\propto (1-x)\gamma(L1) + x\gamma(L2)$, with x the occupation factor for domain walls sited in L_2. This term takes into account that through preferential domain occupation of either L_1 or L_2 regions the magnetostatic energy can be minimized. With the two configurations mixed on an atomic scale, the preferential occupation will favor domain sizes of the order of the local environment size—that is, on an unit cell scale. In consequence, this mechanism would favor narrow domain walls.

In context of the shape memory phenomenon, in the future it will be very interesting to study the influence of disorder for Co_2NbSn and related compounds. To our knowledge, no investigation of the structural and magnetic

properties on a local scale has been carried out for Ni_2MnGa. With the strong stoichiometry dependence of T_S in Ni_2MnGa disorder could be an issue, possibly affecting the characteristics of the martensitic transition. On the other hand, the occurrence of disorder in Co_2NbSn probably reflects a structural instability. The interplay of this structural instability with the band Jahn-Teller induced structural transition will be an interesting topic for future studies.

ACKNOWLEDGMENTS

We acknowledge fruitful discussions with B. Büchner and N.J. Curro, as well as assistance with the SQUID measurements by H. Ahlers and with the specific heat experiments by M. Dischner. This work has been partially supported by the Deutsche Forschungsgemeinschaft DFG under Contract No. SU229/1-1/2 and the European Union Sponsorship.

[1] M. Wuttig, L. Liu, K. Tsuchiya, and R.D. James, J. Appl. Phys. **87**, 4707 (2000).
[2] R.C. O'Handley, S.J. Murry, M. Marioni, H. Nembach, and S.M. Allen, J. Appl. Phys. **87**, 4712 (2000).
[3] K. Inoue, K. Enami, Y. Yamaguchi, K. Ohoyama, Y. Morii, Y. Matsuoka, and K. Inoue, J. Phys. Soc. Jpn. **69**, 3485 (2000).
[4] Y. Ma, S. Awaji, K. Watanabe, M. Matsumoto, and N. Kobayashi, Appl. Phys. Lett. **76**, 37 (2000).
[5] S.-Y. Chu, A. Cramb, M. de Graef, D. Laughlin, and M.E. McHenry, J. Appl. Phys. **87**, 5777 (2000).
[6] P.J. Webster, K.R.A. Ziebeck, S.L. Town, and M.S. Peak, Philos. Mag. B **49**, 295 (1984).
[7] V.A. Chernenko, C. Segui, E. Cesari, J. Pons, and V.V. Kokorin, Phys. Rev. B **57**, 2659 (1998).
[8] P.J. Brown, A.Y. Bargawi, J. Crangle, K.-U. Neumann, and K.R.A. Ziebeck, J. Phys.: Condens. Matter **11**, 4715 (1999).
[9] S. Fujii, S. Ishida, and S. Asano, J. Phys. Soc. Jpn. **58**, 3657 (1989).
[10] M. Terada, Y. Fujita, and K. Endo, J. Phys. Soc. Jpn. **36**, 620 (1974).
[11] K.U. Neumann, T. Kanomata, B. Ouladdiaf, and K.R.A. Ziebeck, J. Phys.: Condens. Matter **14**, 1371 (2002).
[12] A. Yamasaki, S. Imada, R. Arai, H. Utsunomiya, S. Suga, T. Muro, Y. Saitoh, T. Kanomata, and S. Ishida, Phys. Rev. B **65**, 104410 (2002).
[13] D.E. Brandao, M.A. Boff, G.L.F. Fraga, and T.A. Grandi, Phys. Status Solidi A **176**, K45 (1993).
[14] The sample for the resistivity study has been annealed at 800 °C for 7 days, accounting for slightly lower values of $T_C = 112$ K and $T_S = 223$ K.
[15] W. Jeitschko, Metall. Trans. A **1**, 3159 (1972).
[16] For Refs. 10 and 15 the cooling procedures are not specified in detail.
[17] B. Nachumi, Y. Fudamoto, A. Keren, K.M. Kojima, M. Larkin, G.M. Luke, J. Merrin, O. Tchernyshyov, Y.J. Uemura, N. Ichikawa, M. Goto, H. Takagi, S. Uchida, M.K. Crawford, E.M. McCarron, D.E. MacLaughlin, and R.H. Heffner, Phys. Rev. B **58**, 8760 (1998).
[18] J. Rodriguez-Carvajal (unpublished).
[19] A.U.B. Wolter, H.H. Klauss, F.J. Litterst, C. Geibel, and S. Süllow, J. Magn. Magn. Mater. **242-245**, 888 (2002).
[20] R. Skomski and J.M.D. Coey, *Permanent Magnetism* (Institute of Physics Publishing, Bristol, 1999).
[21] C. Mazumdar, R. Nagarajan, L.C. Gupta, B.D. Padalia, and R. Vijayaraghavan, Appl. Phys. Lett. **77**, 895 (2000).
[22] Z. Sun, H. Zhang, J. Wang, and B. Shen, J. Appl. Phys. **86**, 5152 (1999).
[23] K.H.J. Buschow, M. Brouha, and J.B.A.A. Elemans, Phys. Status Solidi A **30**, 177 (1975).
[24] K.H.J. Buschow and M. Brouha, J. Appl. Phys. **47**, 1653 (1976).
[25] S. Süllow, B. Ludoph, C.E. Snel, F.E. Kayzel, E. Brück, G.J. Nieuwenhuys, A.A. Menovsky, and J.A. Mydosh, Z. Phys. B: Condens. Matter **98**, 17 (1995).
[26] M.E. Fisher and J.S. Langer, Phys. Rev. Lett. **20**, 665 (1968).
[27] M.P. Kawatra, S. Skalski, J.A. Mydosh, and J.L. Budnick, Phys. Rev. Lett. **23**, 83 (1969).
[28] N.F. Mott, *Metal Insulator Transitions*, 2nd ed. (Taylor & Francis, London, 1990).
[29] Z.W. Chen, C.L. Lin, T. Mihalisin, and N. Bykowetz, J. Appl. Phys. **73**, 6974 (1993).
[30] A.C. Kunwar, G.L. Turner, and E. Oldfield, J. Magn. Reson. (1969-1992) **69**, 124 (1986).
[31] T.J. Bastow, C.T. Forwood, M.A. Gibson, and M.E. Smith, Phys. Rev. B **58**, 2988 (1998).
[32] J.A. Mydosh, Z. Phys. B: Condens. Matter **103**, 251 (1997); Physica B **259-261**, 882 (2000).
[33] O.O. Bernal, H. Lukefahr, D.E. MacLaughlin, and B. Andraka, Phys. Rev. Lett. **75**, 2023 (1995).
[34] S. Süllow, G.J. Nieuwenhuys, A.A. Menovsky, J.A. Mydosh, S.A.M. Mentink, T.E. Mason, and W.J.L. Buyers, Phys. Rev. Lett. **78**, 54 (1997).
[35] C.E. Booth, D.E. MacLaughlin, R.H. Heffner, M.B. Maple, and G.H. Kwei, Phys. Rev. Lett. **81**, 3960 (1998).
[36] D.X. Li, A. Dönni, Y. Kimura, Y. Shiokawa, Y. Homma, Y. Haga, E. Yamamoto, T. Honma, and Y. Onuki, J. Phys.: Condens. Matter **11**, 8263 (1999).